

# Geometric Limits of Mitotic Pressure Under Confinement

Amit Singh Vishen<sup>1,\*</sup>

<sup>1</sup>Centre for Mechanochemical Cell Biology and Division of Biomedical Sciences,  
Warwick Medical School, University of Warwick, Coventry CV4 7AL, United Kingdom.

(Dated: February 24, 2026)

Cells often divide under mechanical confinement, where surrounding structures restrict shape changes during cytokinesis. Although forces generated during confined division have been measured experimentally, it remains unclear how confinement geometry and mechanics determine the transmitted force. Here we develop a minimal mechanical theory of cell division under confinement. Modeling the cell as an incompressible volume bounded by an interface with effective isotropic tension, we show that confinement restricts the set of mechanically admissible furrow shapes. As the furrow radius decreases, it reaches a confinement-induced minimum. Beyond this point, further ingression does not alter the interface shape, and both pressure and axial force saturate. We analyze force and pressure in rigid, soft, and strong three-dimensional confinement and demonstrate that a single geometric mechanism underlies these distinct cases. After rescaling force and length by the appropriate geometric scale, cells of different size and surface tension collapse onto a single universal curve. The relevant length scale is the cell size for rigid and soft confinement, and the confinement size in fully enclosing three-dimensional confinement. In soft confinement, environmental stiffness and spindle-generated axial forces determine the operating force and pressure, while the geometric constraint fixes the maximal attainable levels. In summary, our results show that mitotic force transmission and mitotic pressure during cytokinesis are bounded by confinement geometry, with material properties and active forces selecting the operating point within these geometry-imposed limits.

## I. INTRODUCTION

Cell division is an intrinsically mechanical process in which internally generated forces reorganize cell shape and partition volume into two daughter compartments [1–3]. In physiological settings, division occurs under mechanical interaction with neighboring cells, tissues, or enclosing structures that constrain possible deformations. The forces generated during division drive tissue morphogenesis and determine whether cells can successfully complete cytokinesis in mechanically restrictive environments such as dense tissues or narrow tissue spaces [4–8]. Understanding how dividing cells generate and transmit forces under confinement is therefore essential for explaining tissue organization, developmental mechanics, and division failure in confined environments.

The mechanical aspects of mitosis have been studied extensively, particularly during mitotic rounding, when cells increase surface tension to regain a nearly spherical shape. Experimental and theoretical work has quantified the pressures associated with rounding and related them to cortical tension and hydrostatic pressure [4, 9–15]. Recent experiments show that dividing cells also exert substantial forces during anaphase and cytokinesis, often exceeding those generated during rounding [16–18]. These measurements establish cytokinesis as the dominant stage of mitotic force production. However, the physical mechanism by which contractile ring activity translates into mitotic pressure and axial force transmission remains unclear.

The difficulty is geometric: the contractile ring generates circumferential tension and contracts radially at the division plane, yet the forces transmitted to confining boundaries act axially, along the division axis. A dividing cell can accommodate radial contraction through shape changes, curvature redistribution, and axial extension, so the relationship between local contractile activity and macroscopic mitotic pressure is not straightforward. How does confinement geometry determine the force output? What is the effect of environmental resistance on the magnitude of transmitted forces? A physical framework connecting ring contraction to mitotic pressure under confinement is currently lacking. Previous theoretical approaches have modeled cytokinesis using active gel descriptions of the cortex and contractile ring dynamics [19–22], but have not addressed how confinement geometry alone constrains admissible shapes and force transmission.

To address these questions, we model the dividing cell as an incompressible fluid enclosed by a membrane–cortex interface with constant effective surface tension and analyze force balance under geometric constraints. This description is closely analogous to classical capillary-bridge problems, in which admissible interface shapes are determined by geometry, incompressibility, and surface tension [11, 15, 23–26].

We characterize cytokinesis by the furrow radius  $R_{\text{div}}$ , defined as the radius of the narrowest cross-section of the membrane–cortex interface at the division plane. Within this framework, we identify two mechanical regimes. During early ingression, admissible interface shapes evolve continuously as the furrow radius decreases, leading to systematic curvature changes and a corresponding

---

\* amit.singh-vishen@warwick.ac.uk

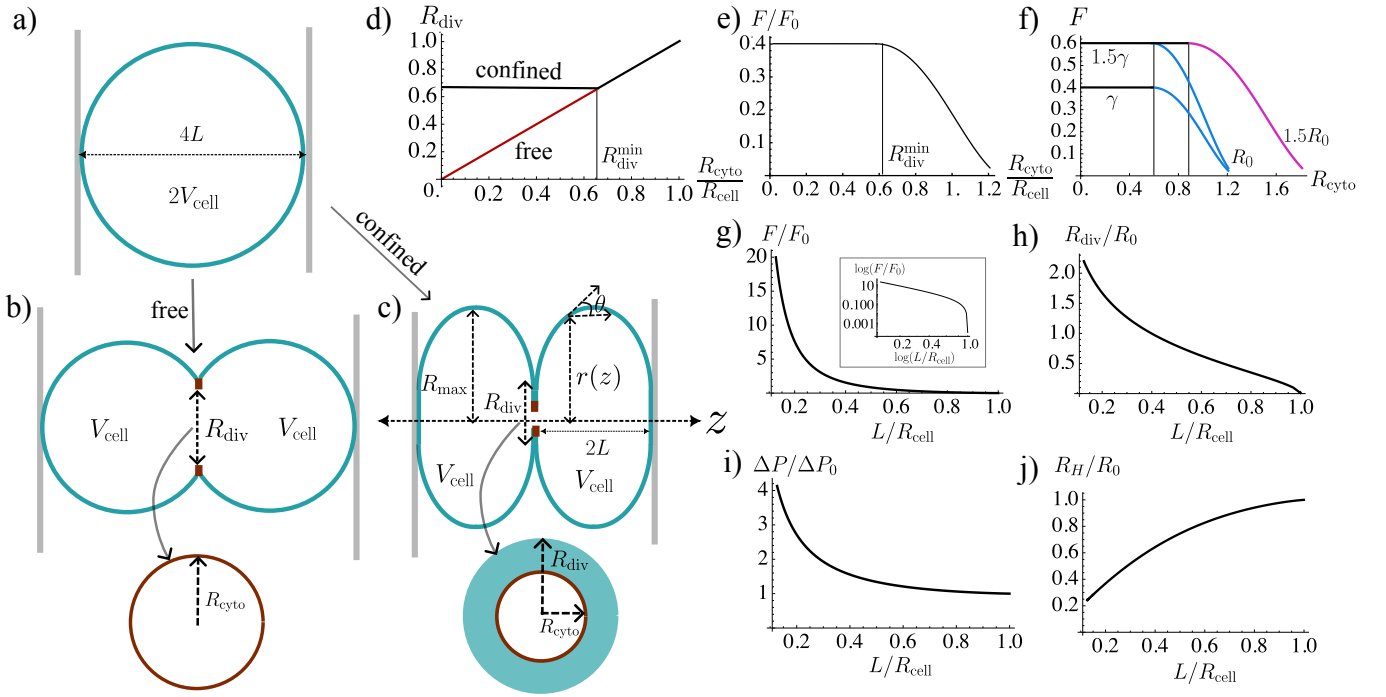


**FIG. 1. Cell division under rigid axial confinement.** (a–c) Schematic of cell division without confinement (free) and between rigid parallel walls (confined). The cell of fixed volume  $2V_{\text{cell}}$  is characterized by the geometric furrow radius  $R_{\text{div}}$  at the division plane and the maximum radius  $R_{\max}$ . Under confinement, axial elongation is restricted by the wall separation  $4L$ . (d) Geometric furrow radius  $R_{\text{div}}$  as a function of cytokinetic ring radius  $R_{\text{cyto}}$ . In the absence of confinement,  $R_{\text{div}} \simeq R_{\text{cyto}}$ . Under confinement,  $R_{\text{div}}$  saturates at the confinement-induced minimum  $R_{\text{div}}^{\min}$ . (e) Dimensionless axial force  $F/F_0$  as a function of furrow radius. The force increases during ingestion and saturates once  $R_{\text{div}}^{\min}$  is reached. (f) Axial force in physical units for different cell radii and surface tensions. Increasing cell size at fixed tension changes the minimum furrow radius but not the saturating force, whereas increasing tension at fixed cell size rescales the force without affecting the minimum furrow radius. (g) Scaled saturation force  $F/F_0$  as a function of dimensionless wall separation  $L/R_{\text{cell}}$  for fixed cell volume. (h) Confinement-induced minimum furrow radius  $R_{\text{div}}/R_{\text{cell}}$  as a function of  $L/R_{\text{cell}}$ . (i) Scaled saturation pressure difference  $\Delta P/\Delta P_0$  as a function of  $L/R_{\text{cell}}$ . (j) Radius of curvature at saturation  $R_H/R_{\text{cell}}$  as a function of  $L/R_{\text{cell}}$ . Here  $F_0 = 2\pi\gamma R_{\text{cell}}$  is the characteristic force scale, and  $\Delta P_0 = 2\gamma/R_{\text{cell}}$  is the corresponding pressure scale.

increase in mitotic pressure. This evolution persists until the furrow radius reaches a confinement-induced minimum set by geometric constraints. Beyond this point, further ingestion does not modify the interface shape. As a consequence, mitotic pressure saturates, and cytokinesis proceeds through septum-like closure at essentially constant pressure.

We analyze a hierarchy of confinement geometries: rigid, soft, and cylindrical confinement. Rigid axial confinement determines the admissible interface shapes and how mitotic pressure evolves with furrow ingestion. Soft confinement is modeled as a deformable environment with finite stiffness and selects the operating force through force balance, making explicit how mitotic pressure depends on environmental mechanics. We then consider cylindrical confinement, in which both axial and radial deformations are restricted and the cylinder radius sets the relevant geometric length scale. Forces generated by the mitotic spindle are included as additional axial driving terms in the force balance. These forces alter the magnitude of mitotic pressure and the furrow radius at

which saturation occurs, but do not change the qualitative geometric constraints imposed by confinement.

## II. RIGID AXIAL CONFINEMENT

We begin by analyzing cell division under rigid confinement in order to establish the mechanical and geometric framework used throughout this work. We consider a dividing animal cell of fixed volume  $2V_{\text{cell}} = 8\pi R_{\text{cell}}^3/3$ , where  $R_{\text{cell}}$  is the radius of sphere of volume equal to cell volume after division. The cell is confined between two parallel, rigid walls separated by a fixed distance  $4L$  (Fig. 1(a)). The cell is modeled as an incompressible fluid enclosed by a membrane-cortex interface with constant effective surface tension  $\gamma$ . Active processes associated with cytokinesis, such as actomyosin contractility, are not modeled explicitly; instead, the radius of the cytokinetic ring  $R_{\text{cyto}}$  is treated as an externally prescribed input parameter.

A key distinction in the following is between the cy-

tokinetic ring radius  $R_{\text{cyto}}$  and the geometric furrow radius  $R_{\text{div}}$ , defined as the radius of the cross-section of the membrane–cortex interface at the division plane. As we show below, while  $R_{\text{cyto}}$  may decrease continuously during cytokinesis and can in principle approach zero, the furrow radius  $R_{\text{div}}$  is constrained by geometry and confinement and need not follow  $R_{\text{cyto}}$  once the confinement-induced minimum furrow radius set by geometric constraints is reached (Fig. 1(b-d)).

The cell shape is assumed to be axisymmetric about the division axis  $z$  and is described by a local radius  $r(z)$ . Mechanical equilibrium requires force balance across any cross-section perpendicular to the division axis. In the presence of a compressive force  $F$  exerted by the confining walls, this balance reads [26, 27]

$$2\pi r \cos \theta - \pi r^2 \Delta P + F = 0, \quad (1)$$

where  $\theta$  is the angle between the membrane tangent and the division axis. Positive  $F$  corresponds to compression by the walls. The pressure difference is related to the curvature through the Young-Laplace law:  $\Delta P = 2\gamma/R_H$ , where  $R_H$  is the radius of curvature. Introducing the force length scale  $R_F = F/(2\pi\gamma)$ , Eq. (1) can be written as a quadratic equation for the local radius  $r$  [26],

$$r^2 - R_H r \cos \theta - R_H R_F = 0. \quad (2)$$

Solving this equation yields two branches,

$$r_{\pm} = \frac{R_H \cos \theta \pm \sqrt{R_H^2 \cos^2 \theta + 4R_H R_F}}{2}. \quad (3)$$

For compressive confinement ( $R_F > 0$ ), only the positive branch corresponds to a physical solution. We can solve for the shape of the cell for given  $R_H$  and  $R_F$  by parametrize the shape by arch length  $s$  and imposing the appropriate boundary conditions (see Appendix A).

The maximum cell radius occurs where the surface tangent is parallel to the division axis ( $\theta = 0$ ). At the division plane, the angle is controlled by the dynamics of cytokinetic ring. The minimum radius occurs when the surface tangent is perpendicular to the division axis ( $\theta = \pi/2$ ). From Eq. (3) the confinement-imposed minimum furrow radius at  $\theta = \pi/2$  is

$$R_{\text{div}}^{\min} = \sqrt{R_H R_F}. \quad (4)$$

The geometric furrow radius therefore satisfies

$$R_{\text{div}} = \max(R_{\text{cyto}}, R_{\text{div}}^{\min}). \quad (5)$$

For  $R_{\text{cyto}} > R_{\text{div}}^{\min}$ , the interface follows ring constriction and  $R_{\text{div}} \simeq R_{\text{cyto}}$ . Once  $R_{\text{cyto}}$  reaches  $R_{\text{div}}^{\min}$ , further ring contraction does not lead to additional furrow ingression (Fig. 1(d)).

The two unknowns  $R_F$  and  $R_H$  are determined by imposing the two constraints: given confinement separation  $L$ , and constant volume  $V_{\text{cell}}$  (see Appendix A).

We nondimensionalise the problem by scaling all lengths by the undeformed cell radius  $R_{\text{cell}}$  and all forces by the scale  $F_0 = 2\pi\gamma R_{\text{cell}}$ . With this choice, the cell volume is fixed to  $V_{\text{cell}}/R_{\text{cell}}^3 = 4\pi/3$ , and the model reduces to a single dimensionless control parameter,  $l = L/R_{\text{cell}}$ . In this rescaled formulation, the cell shape, furrow geometry, and mean curvature are fully determined by  $l$  and are independent of both the absolute cell size and the surface tension. Physical forces are recovered by restoring the force scale, implying that under geometrically similar confinement larger cells generate proportionally larger forces while exhibiting identical dimensionless shapes. Importantly, both the radius of curvature and the minimum furrow radius are independent of the surface tension and are set solely by geometric constraints.

Figure 1(f) illustrates the distinct roles of cell size and surface tension. Varying the cell size shifts the minimum attainable furrow radius without affecting the saturating force, whereas varying the surface tension changes the saturating force while leaving the minimum furrow radius unchanged.

The scaled saturation force and the confinement-induced minimum furrow radius are shown as functions of the dimensionless confinement parameter  $l$  in Figs. 1(g) and 1(h), respectively. The corresponding scaled pressure difference and radii of curvature are plotted in Figs. 1(i) and 1(j). In dimensionless form, both the geometry and the curvature are determined entirely by  $l$ , independent of cell size and surface tension. Restoring physical units provides representative force and pressure magnitudes. For  $\gamma \approx 1 \text{ mN/m}$  [11] and  $R_{\text{cell}} \approx 10 \mu\text{m}$ , the associated characteristic scales are  $F_0 = 2\pi\gamma R_{\text{cell}} \approx 60 \text{ nN}$  and  $\Delta P_0 = 2\gamma/R_{\text{cell}} \approx 200 \text{ Pa}$ . A cell dividing at  $l = 0.5$  generates an axial force of about 50 nN and an internal pressure of about 250 Pa.

### III. SOFT AXIAL CONFINEMENT

So far we have imposed a fixed length  $L$  between the confining walls. In biological contexts such as tissues and epithelia, the environment is deformable rather than rigid. To understand the effect of deformability of the environment on the mitotic pressure, we now study cell division under soft confinement.

We model the surrounding environment as a deformable confinement characterized by an effective elastic stiffness  $k$ . At a coarse-grained level, the resistance of the environment to deformation by the dividing cell is described by a linear force–displacement relation,

$$F_{\text{env}}(X) = k(X_{\text{ref}} - X), \quad (6)$$

where  $X$  is the instantaneous spring length and  $X_{\text{ref}}$  is the reference length. Here  $F_{\text{env}}(X)$  is the force on the cell by the surrounding tissue. We can express  $X$  in terms of  $L$ . For the configuration in Fig. 2(a) we get  $F_{\text{env}}(L) = k(L_0 - L)$ .

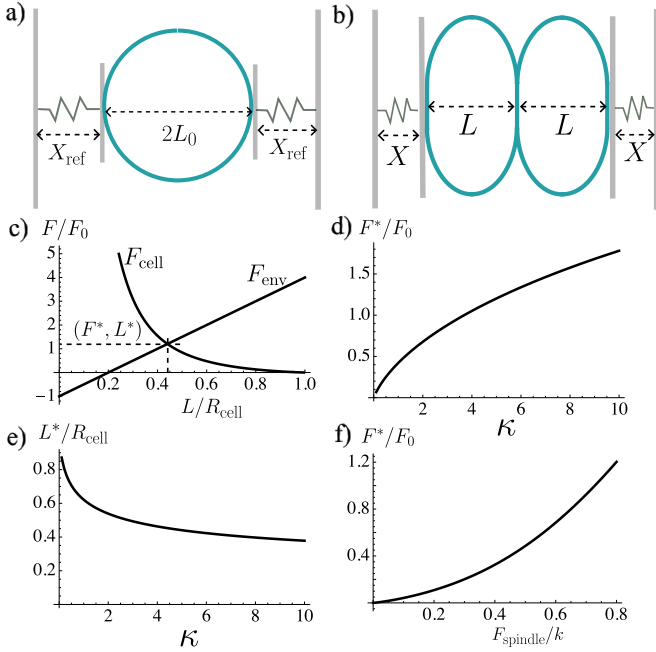


**FIG. 2. Cell division under soft confinement.** (a–b) Schematic of soft axial confinement modeled as an elastic element of stiffness  $k$ . During cytokinesis, furrow ingression elongates the cell along the division axis and compresses the surrounding medium. (c) Graphical construction of mechanical equilibrium. The axial force generated by the cell under rigid confinement,  $F_{\text{cell}}(L)$ , is shown together with the elastic force-length relation of the environment,  $F_{\text{env}}(L)$ . The operating point  $(L^*, F^*)$  is given by the intersection of the two curves. Increasing stiffness  $\kappa$  steepens the environmental response and shifts the equilibrium toward smaller separations and larger forces. In the limit  $\kappa \rightarrow \infty$ , the solution approaches the rigid-wall limit. (d) Equilibrium force  $F^*$  as a function of stiffness  $\kappa$ . (e) Equilibrium cell half-length  $L^*$  as a function of stiffness. (f) Equilibrium force  $F^*$  as a function of spindle-generated axial force, showing shifts of the operating point along the force-geometry relation.

The rigid-wall analysis provides a constitutive relation  $F_{\text{cell}}(L)$  between the force transmitted by the cell and the confinement length at fixed cell volume (Fig. 1(a)). Mechanical equilibrium under soft confinement is obtained from the condition

$$F_{\text{cell}}(L^*) = F_{\text{env}}(L^*), \quad (7)$$

so that the operating point  $(L^*, F^*)$  is given by the intersection of the rigid-wall force-geometry relation with the elastic force-length relation of the environment Fig. 2(c).

It is convenient to introduce a dimensionless measure of confinement stiffness,  $\kappa = k/2\pi\gamma$ . The parameter  $\kappa$  compares the elastic resistance of the environment to the intrinsic force scale set by membrane tension. For  $\kappa \ll 1$ , confinement weakly perturbs furrow closure and forces remain small. As  $\kappa$  increases, the confinement-limited minimum furrow radius is reached at progressively larger forces, and the system continuously approaches the rigid-

wall force-displacement relation (Fig. 2(c–e)).

In addition to confinement, active forces generated by the mitotic spindle contribute to the axial force balance during cytokinesis. Within the present framework, the total axial force on the cell is

$$F = F_{\text{env}} + F_{\text{spindle}}, \quad (8)$$

where  $F_{\text{env}}$  is the reaction force arising from confinement and  $F_{\text{spindle}}$  represents spindle-generated forces acting along the division axis. Since the spindle forces push on the confinement  $F_{\text{spindle}} < 0$ . Fig. 2(f) shows axial saturation force as a function spindle force.

Spindle forces enter additively in the force balance and therefore shift the operating point along the force-geometry relation determined by confinement. The effect of a constant spindle force can be included in the model by redefining the rest length of the spring as  $X'_{\text{ref}} = X_{\text{ref}} + F_{\text{spindle}}/k$ .

The intrinsic force and pressure scales remain  $F_0 = 2\pi\gamma R_{\text{cell}}$  and  $\Delta P_0 = 2\gamma/R_{\text{cell}}$ . For  $\gamma \sim 0.1\text{--}1\text{ mN/m}$  and  $R_{\text{cell}} \sim 10\text{ }\mu\text{m}$ , these correspond to  $F_0 \sim 6\text{--}60\text{ nN}$  and  $\Delta P_0 \sim 20\text{--}200\text{ Pa}$ . If confinement is provided by neighboring cells whose mechanics are dominated by cortical tension  $\gamma_{\text{env}}$ , the effective restoring stiffness scales as  $k \sim 2\pi\gamma_{\text{env}}$  [28], yielding  $\kappa \sim \gamma_{\text{env}}/\gamma$ . For a mitotic cell whose tension exceeds that of its neighbors by a factor of a few, one expects  $\kappa \sim 0.1\text{--}0.3$ , so that  $F^* \sim \kappa F_0$  lies in the range of a few nanonewtons, consistent with measured axial forces of 1–10 nN during confined cytokinesis [16].

#### IV. CONFINEMENT IN A CYLINDER WITH HEMISPHERICAL CAPS

Thus far, confinement was treated primarily as one-dimensional, as in the parallel-wall geometry. In many biological and experimental settings, however, dividing cells experience three-dimensional confinement that restricts both axial and radial deformations, such as in eggshells, compact tissues, or microfluidic channels. We therefore examine how global three-dimensional confinement controls force generation during cytokinesis.

We consider a cell dividing inside a rigid cylindrical chamber of radius  $R_{\text{cyl}}$  and total length  $L_{\text{cyl}}$ , closed at both ends by hemispherical caps Fig. 3(a). Confinement requires that the radius  $R_{\text{cell}}$  of the equal-volume unconfined spherical cell satisfies  $R_{\text{cell}} > R_{\text{cyl}}$ . As a result, the cell is radially confined throughout division and its maximum radius is fixed to  $R_{\text{max}} = R_{\text{cyl}}$ . Radial confinement therefore implies a nonzero normal stress on the cylindrical wall. Prior to contact with the hemispherical caps, the dominant curvature scale is set by  $R_{\text{cyl}}$ , and the pressure is given by  $\Delta P = 2\gamma/R_{\text{cyl}}$ .

If the cell contacts the cylinder over an axial length  $L_{\text{contact}}$ , the total radial force exerted on the cylindrical wall scales as

$$F_{\text{rad}}/F_0 = 2L_{\text{contact}}/R_{\text{cyl}}, \quad (9)$$

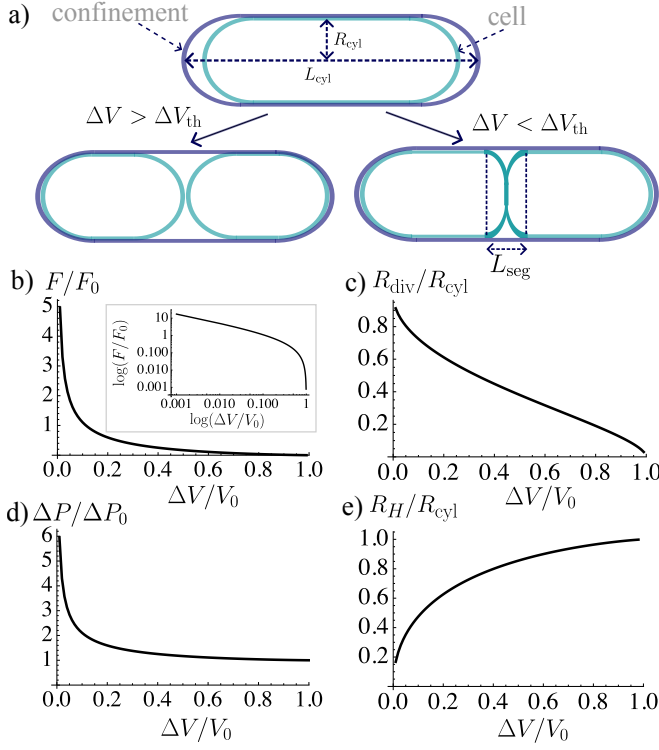


**FIG. 3. Cell division under cylindrical confinement.** (a) Geometry of a cell confined within a cylindrical chamber of radius  $R_{\text{cyl}}$  and length  $L_{\text{cyl}}$ , with hemispherical caps. Two regimes are shown: for excess free volume  $\Delta V > \Delta V_{\text{th}}$  the cell accommodates division by axial elongation without transmitting axial force; for  $\Delta V < \Delta V_{\text{th}}$ , ingression requires pushing against the caps, leading to nonzero axial force. (b) Dimensionless axial force at saturation  $F/F_0$  as a function of reduced free volume  $\Delta V/V_0$ . The inset shows the same relation on logarithmic scales. (c) Furrow radius at saturation  $R_{\text{div}}/R_{\text{cyl}}$  as a function of  $\Delta V/V_0$ , illustrating pinning at a confinement-induced minimum. (d) Scaled saturation pressure  $\Delta P/\Delta P_0$  as a function of  $\Delta V/V_0$ , showing saturation in the confinement-limited regime. (e) Radius of curvature at saturation  $R_H/R_{\text{cyl}}$  as a function of  $\Delta V/V_0$ . Here  $V_0 \equiv 2\pi R_{\text{cyl}}^3/3$  is the reference volume,  $F_0 = 2\pi\gamma R_{\text{cyl}}$  is the characteristic force scale under cylindrical confinement, and  $\Delta P_0 = 2\gamma/R_{\text{cyl}}$  is the corresponding pressure scale.

where  $F_0 \equiv 2\pi\gamma R_{\text{cyl}}$ . In this regime, the axial compressive force on the hemispherical caps remains zero.

The total available volume inside the chamber is

$$V_{\text{cyl}} = \pi R_{\text{cyl}}^2 (L_{\text{cyl}} - 2R_{\text{cyl}}) + \frac{4}{3}\pi R_{\text{cyl}}^3,$$

and we define the excess (free) volume

$$\Delta V = V_{\text{cyl}} - V_{\text{cell}}, \quad (10)$$

which quantifies the space available to accommodate shape changes during division. The axial force transmitted along the division axis is controlled by this available free volume  $\Delta V$ . As  $\Delta V$  is reduced, axial elongation becomes progressively restricted. Once the cell surface

comes into contact with the hemispherical caps, axial force transmission becomes unavoidable. This occurs below a threshold free volume

$$\Delta V_{\text{th}} = \frac{2\pi}{3} R_{\text{cyl}}^3.$$

Beyond this point, the surface between the division plane and the cap contact point separates into a contact region, where the geometry is imposed by the confinement, and a free segment not in contact with the chamber. This free segment extends from the division plane ( $r = R_{\text{div}}$ ) to the detachment point from the cylinder and obeys the force-balance condition given by Eq. (2). Evaluating the force balance at the detachment point by substituting  $r = R_{\text{cyl}}$  and  $\theta = 0$  in Eq. (2) yields

$$\frac{R_F}{R_{\text{cyl}}} = \left( \frac{R_{\text{cyl}}}{R_H} - 1 \right), \quad (11)$$

which relates the axial force transmitted to the caps to the curvature radius of the free segment.

The curvature radius  $R_H$  is determined by enforcing volume conservation for the free segment. Denoting by  $L_{\text{seg}}(R_H)$  its axial extent and by  $V_{\text{seg}}(R_H)$  its volume, volume conservation requires

$$\pi R_{\text{cyl}}^2 L_{\text{seg}}(R_H) - V_{\text{seg}}(R_H) = \Delta V. \quad (12)$$

This condition fixes  $R_H$  self-consistently and thereby determines the axial force and the minimum attainable furrow radius. For a given  $\Delta V$ , admissible constant-curvature configurations evolve with decreasing  $R_{\text{div}}$  until the minimum furrow radius is reached. Beyond this point, further ring contraction does not modify the interface shape, and both axial force and internal pressure saturate. The saturation force is obtained by substituting  $R_{\text{div}} = R_{\text{div}}^{\min}$  into Eq. (12).

Cylindrical confinement admits a natural dimensionless formulation obtained by scaling all lengths by the confining radius  $R_{\text{cyl}}$  and all forces by the scale  $F_{\text{cyl}} = 2\pi\gamma R_{\text{cyl}}$ . With this choice, the geometry of the chamber fixes the curvature scale, and the problem reduces to a single effective control parameter, the dimensionless free volume  $\Delta V/V_0$ , where  $V_0 = 2\pi R_{\text{cyl}}^3/3$ . In this rescaled description, the cell shape, interface curvature, and confinement-limited furrow radius are fully determined by  $\Delta V/V_0$  and are independent of the intrinsic cell size and surface tension.

This behavior contrasts with axial confinement, where the cell radius sets the geometric scale and the force grows proportionally with cell size. Under cylindrical confinement, the environment replaces the cell as the dominant geometric scale, highlighting the central role of free volume and three-dimensional confinement geometry in controlling axial compression during cytokinesis.

The resulting force-volume, pressure-volume, and force-radius relations are shown in Fig. 3(b–e). In the confinement-limited regime, the furrow radius, internal pressure, and axial force collapse onto geometry-controlled plateaus set by  $R_{\text{cyl}}$ . Restoring physical units provides representative force and pressure magnitudes.

## V. DISCUSSION

We have identified a geometry-induced minimum furrow radius as the key mechanical constraint governing mitotic pressure under confinement. In this framework, contractile ring activity increases curvature and pressure only while the interface can change shape. Once the confinement-induced minimum is reached, further ring contraction no longer alters the interface geometry, and both pressure and transmitted force saturate. Mitotic pressure therefore reflects not only active contractility, but also the interaction between contractile forces and confinement-restricted shape.

This mechanism provides a physical explanation for septum-like closure in confined environments. While septation can arise in unconfined constant-tension models through internal geometric constraints [29], external confinement introduces an additional and independent restriction. Under confinement, septum-like division emerges naturally once admissible shapes are exhausted, without invoking detailed assumptions about ring mechanics.

In soft confinement, increasing environmental stiffness shifts the operating pressure while leaving the minimum furrow radius unchanged. Spindle-generated forces enter additively in the axial force balance and similarly shift the pressure level and the onset of saturation, but they do not remove the confinement-induced constraint on shape. Geometry defines the allowable range of pressure; material properties and active forces select an operating point within that range.

Under strong three-dimensional confinement, the confining diameter replaces cell size as the relevant geometric scale. Once radial confinement is saturated, curvature is fixed by chamber geometry, and axial force becomes independent of intrinsic cell size. This provides a mechanical explanation for the amplification of mitotic forces observed in narrow channels and dense tissues.

The model assumes incompressibility, effective isotropic surface tension, and quasistatic force balance. These simplifications isolate geometric effects but neglect viscous dissipation and active cortical remodeling. Incorporating such dynamics will be necessary to describe the full time evolution of cytokinesis [19, 20]. Nevertheless, the geometry-induced minimum furrow radius identified here represents a robust mechanical constraint that should persist beyond the present approximations.

Constant-tension descriptions of confined interfaces are, in principle, unstable to off-center perturbations, since displacement of the division plane generates asymmetric curvatures and Laplace pressures. In living cells, however, the contractile ring is actively positioned and stabilized by spindle-mediated cues and cortical patterning [30]. Ring positioning can therefore be regarded as a fast, actively controlled degree of freedom that maintains midplane symmetry, while slower geometric constraints determine the admissible interface shapes and resulting pressure.

The present framework assumes constant cell volume during cytokinesis. Animal cells exhibit volume changes across the cell cycle [31, 32]. In a quasistatic approximation, slow volume changes can be incorporated by treating total volume as a slowly varying parameter, which shifts the force-geometry relation without altering the existence of a confinement-induced minimum furrow radius. The geometry-induced saturation mechanism therefore persists provided volume changes remain gradual compared to mechanical relaxation.

The framework yields clear experimental predictions. Under strong three-dimensional confinement, force and pressure should scale with the confining diameter rather than cell size. In deformable environments, increasing stiffness should shift the operating point without altering the geometry-induced saturation plateau. Perturbing spindle forces should change the pressure level at which saturation occurs while preserving the minimum furrow radius set by geometric constraints.

## VI. ACKNOWLEDGMENT

ASV acknowledges funding from Leverhulme Trust (LIP-2021-017).

## Appendix A: Shape under confinement

We derive the shape of a confined dividing cell assuming axisymmetry and constant surface tension. The cell surface is modeled as a constant-mean-curvature (CMC) surface enclosing an incompressible fluid [11, 24–26].

The surface is parametrized by arc length  $s$  and local radius  $r(s)$ , with  $\theta(s)$  the angle between the surface tangent and the axis of symmetry. We choose  $s = 0$  at the point of maximum radius  $r = R_{\max}$ , where  $\theta = 0$ . The division plane (furrow) and the confining wall correspond to arc-length positions  $s = s_d$  and  $s = s_w$ , respectively. From Eq. (2),

$$\cos \theta = \frac{r}{R_H} - \frac{R_F}{r}, \quad (\text{A1})$$

and using  $dr/ds = \sin \theta$ , we obtain

$$\left( \frac{dr}{ds} \right)^2 = 1 - \left( \frac{r}{R_H} - \frac{R_F}{r} \right)^2 = \frac{(R_{\max}^2 - r^2)(r^2 - r_{\min}^2)}{R_H^2 r^2}, \quad (\text{A2})$$

with turning points

$$R_{\max,\min} = \frac{R_H}{2} \left( 1 \pm \sqrt{1 + 4 \frac{R_F}{R_H}} \right). \quad (\text{A3})$$

For compressive confinement ( $R_F > 0$ ),  $r_{\min} < 0$  and does not represent a physical radius; it is retained as a formal parameter that simplifies the integration.

Introducing the dimensionless variable  $u = s/R_H$  and the parameter

$$\alpha = 1 - \left( \frac{r_{\min}}{R_{\max}} \right)^2, \quad (\text{A4})$$

Eq. (A2) integrates to the standard CMC profile

$$r(s) = R_{\max} \sqrt{1 - \alpha \sin^2 u}. \quad (\text{A5})$$

The axial coordinate follows from  $dz/ds = \cos \theta$ . Substituting Eq. (A1) and integrating yields

$$z(s) = R_H \left[ \frac{R_{\max}}{R_H} \mathbb{E}(u, \alpha) - \frac{R_F}{R_{\max}} \mathbb{F}(u, \alpha) \right], \quad (\text{A6})$$

where  $\mathbb{F}$  and  $\mathbb{E}$  are the incomplete elliptic integrals of the first and second kind, respectively, and  $z(0) = 0$  at  $r = R_{\max}$ .

The arc-length positions  $s_d$  and  $s_w$  are obtained from Eq. (A5) by setting  $r = R_{\text{div}}$  and  $r = R_w$ , respectively. The half-length of the confined cell is

$$L = z(s_d) + z(s_w), \quad (\text{A7})$$

so that the total axial extent is  $2L$ . The enclosed volume between the division plane and the wall is  $V = V(s_d) + V(s_w)$ , where

$$V(s) = \pi \int_0^s r^2(s) \frac{dz}{ds} ds. \quad (\text{A8})$$

This integral can be expressed in closed form using elliptic integrals. For a given confinement geometry and applied force, the curvature radius  $c R_H$  is determined self-consistently by imposing volume conservation.

- 
- [1] C. Guillot and T. Lecuit, *Dev. Cell* **24**, 227 (2013).  
[2] J. M. Scholey, I. Brust-Mascher, and A. Mogilner, *Nature* **422**, 746 (2003).  
[3] T. D. Pollard and B. O'Shaughnessy, *Annu. Rev. Biochem.* **88**, 661 (2019).  
[4] C. J. Cattin, M. Düggelin, D. Martinez-Martin, C. Gerber, D. J. Müller, and M. P. Stewart, *Proc. Natl. Acad. Sci. U.S.A.* **112**, 11258 (2015).  
[5] P. Campinho, M. Behrndt, J. Ranft, T. Risler, N. Minc, and C.-P. Heisenberg, *Nat. Cell Biol.* **15**, 1405 (2013).  
[6] M. F. Wang, M. V. Hunter, G. Wang, C. McFaul, C. M. Yip, and R. Fernandez-Gonzalez, *Development* **144**, 1350 (2017).  
[7] Z. Tang, Y. Hu, Z. Wang, K. Jiang, C. Zhan, W. F. Marshall, and N. Tang, *Dev. Cell* **44**, 313 (2018).  
[8] N. Tarannum, R. Singh, and S. Woolner, *J. Dev. Biol.* **10**, 37 (2022).  
[9] M. P. Stewart, J. Helenius, Y. Toyoda, S. P. Ramanathan, D. J. Muller, and A. A. Hyman, *Nature* **469**, 226 (2011).  
[10] S. P. Ramanathan, J. Helenius, M. P. Stewart, C. J. Cattin, A. A. Hyman, and D. J. Muller, *Nat. Cell Biol.* **17**, 148 (2015).  
[11] E. Fischer-Friedrich, A. A. Hyman, F. Jülicher, D. J. Müller, and J. Helenius, *Sci. Rep.* **4**, 6213 (2014).  
[12] B. Sorice, C. Escobedo, Y. Toyoda, M. P. Stewart, C. J. Cattin, R. Newton, I. Banerjee, A. Stettler, B. Roska, S. Eaton, A. A. Hyman, A. Hierlemann, and D. J. Müller, *Nat. Commun.* **6**, 8872 (2015).  
[13] O. M. Lancaster, M. Le Berre, A. Dimitracopoulos, D. Bonazzi, E. Zlotek-Zlotkiewicz, R. Picone, T. Duke, M. Piel, and B. Baum, *Dev. Cell* **25**, 270 (2013).  
[14] A. V. Taubenberger, B. Baum, and H. K. Matthews, *Front. Cell Dev. Biol.* **8**, 687 (2020).  
[15] Y. Yang and H. Jiang, *Biophys. J.* **120**, 2306 (2021).  
[16] S. Nam and O. Chaudhuri, *Nat. Phys.* **14**, 621 (2018).  
[17] V. K. Gupta, S. Nam, D. Yim, J. Camuglia, J. L. Martin, E. N. Sanders, L. E. O'Brien, A. C. Martin, T. Kim, and O. Chaudhuri, *J. Cell Biol.* **220**, e202011106 (2021).  
[18] S. Nam, Y.-H. Lin, T. Kim, and O. Chaudhuri, *Adv. Sci.* **8**, 2000403 (2021).  
[19] H. Turlier, B. Audoly, J. Prost, and J.-F. Joanny, *Biophys. J.* **106**, 114 (2014).  
[20] G. Salbreux and F. Jülicher, *Phys. Rev. E* **96**, 032404 (2017).  
[21] J. F. Dorn, L. Zhang, T.-T. Phi, B. Lacroix, P. S. Maddox, J. Liu, and A. S. Maddox, *Mol. Biol. Cell* **27**, 1286 (2016).  
[22] M. Chatterjee, A. Chatterjee, A. Nandi, and A. Sain, *Phys. Rev. Lett.* **128**, 068102 (2022).  
[23] M. Yoneda and K. Dan, *J. Exp. Biol.* **57**, 575 (1972).  
[24] F. Brochard-Wyart and P.-G. de Gennes, *C. R. Phys.* **4**, 281 (2003).  
[25] Y. Yang and H. Jiang, *Phys. Rev. Lett.* **118**, 208102 (2017).  
[26] A. S. Vishen, J. Prost, and P. Sens, *Eur. Phys. J. E* **47**, 22 (2024).  
[27] F. Brochard-Wyart and P.-G. de Gennes, *Proc. Natl. Acad. Sci. U.S.A.* **99**, 7854 (2002).  
[28] E. Hannezo, J. Prost, and J.-F. Joanny, *Proc. Natl. Acad. Sci. U.S.A.* **111**, 27 (2014).  
[29] A. Sain, M. M. Inamdar, and F. Jülicher, *Phys. Rev. Lett.* **114**, 048102 (2015).  
[30] R. A. Green, E. Paluch, and K. Oegema, *Annu. Rev. Cell Dev. Biol.* **28**, 29 (2012).  
[31] C. Cadart, E. Zlotek-Zlotkiewicz, M. Le Berre, M. Piel, and H. K. Matthews, *Dev. Cell* **29**, 159 (2014).  
[32] E. Zlotek-Zlotkiewicz, S. Monnier, G. Cappello, M. Le Berre, and M. Piel, *J. Cell Biol.* **211**, 765 (2015).